

The quasi-geostrophic model for rapidly rotating spherical convection outside the tangent cylinder

By N. GILLET¹† AND C. A. JONES²

¹Laboratoire de Géophysique Interne et Tectonophysique, Observatoire de Grenoble,
B.P. 53, 38041 Grenoble, France

²Department of Applied Mathematics, University of Leeds, Leeds, LS2 9JT, UK

(Received 3 May 2005 and in revised form 13 October 2005)

Rapidly rotating convection in spherical geometry outside the tangent cylinder is investigated using the quasi-geostrophic approximation. The validity of the approximation is discussed, and numerical simulations using these equations are performed, reaching Ekman numbers, E , down to 10^{-6} . The results are compared with experiments and fully three-dimensional numerical simulations. We find that the inertial scaling developed to study rapidly rotating convection does not represent the Prandtl-number dependence of our results adequately. Instead, we find that even in strongly supercritical situations the dominant wavenumbers at the onset of convection still have a strong influence on the behaviour. We find that the local Péclet number, the product of the typical convective velocity and local convective length scale divided by the thermal diffusivity, is helpful for understanding the dynamics of rapidly rotating convection. We explore the zonal flows driven by Reynolds stresses with no-slip boundaries and explore their Prandtl-number dependence. We also study the convective heat transport at low E , and consider the boundary layer structures that can form at large Rayleigh number, slowing down the rate of growth of the Nusselt number with Rayleigh number.

1. Introduction

The onset of convection in rapidly rotating spherical systems is now fairly well-understood (Roberts 1968; Busse 1970; Jones, Soward & Mussa 2000; Dormy *et al.* 2004). As expected from the Taylor–Proudman constraint for slow steady motions in rotating fluids, columnar structures are generally preferred. An exception is the case of very low-Prandtl-number convection (Zhang 1995) where very fast inertial modes, oscillating on the rotation frequency time scale, may dominate over columnar convection which oscillates on a time scale a factor $O(E^{-1/3})$ longer. This very low-Prandtl-number regime has received much attention recently (Ardes, Busse & Wicht 1997; Herrmann & Busse 1997; Plaut & Busse 2002; Busse & Simitev 2004). Here we consider only the columnar regime, which appears to dominate in the experiments of Aubert *et al.* (2001) even at the Prandtl number of liquid gallium, $P = 0.025$.

Many laboratory experiments on rapidly rotating spherical systems have been performed, using a variety of working fluids. These all have sufficiently high rotation rates for the centrifugal acceleration to dominate over gravity. Pioneering work was done by Busse & Carrigan (1976), Carrigan & Busse (1983), Azouni, Bolton &

† Present address: Department of Earth Sciences, University of Leeds, Leeds, LS2 9JT, UK.

Busse (1986), Hart, Glatzmaier & Toomre (1986), Cardin & Olson (1992, 1994) and Manneville & Olson (1996), in which the columnar form of convection was established and the formation of zonal flows investigated. Cordero & Busse (1992) and Cordero (1993) investigated experimentally the behaviour near critical. More recently, Aubert *et al.* (2001) used a configuration in which a spherical container with a cylindrical ‘inner core’ is rapidly rotated. The inner cylinder is cooled relative to the outer sphere, leading to thermal convection in the fluid. Both the water ($P = 7$) and gallium cases have been investigated. A different configuration has been used by Sumita & Olson (2000, 2003) in which a hemispherical inner core is enclosed by a hemispherical outer boundary, with a rigid flat lid at the equator. Thermal convection is induced by cooling the inner hemisphere relative to the outer sphere. A third configuration, in which a spherical inner core is held in place inside a spherical outer sphere by means of rigid rods through which the coolant is pumped, is currently being investigated by Shew (Shew, Sisan & Lathrop 2002; Shew 2004). All these experiments have Ekman number $E = \nu/\Omega d^2$, ν being the kinematic viscosity, Ω the rotation rate and d the gap width between the spherical shells, in the range 10^{-5} – 10^{-7} . The radius ratio of the outer sphere (or hemisphere) to the inner sphere (or cylinder) is typically between 0.3 and 0.4. A wide range of Rayleigh numbers is attainable, up to 600 times critical in the case of the Sumita & Olson (2003) experiment, though none of these experiments are suitable for the study of convection near onset.

An analysis of the experimental results led Aubert *et al.* (2001) and Aubert, Gillet & Cardin (2003) to propose that rapidly rotating columnar convection is frequently in an inertial regime, in which there is a balance between Coriolis force, buoyancy force and inertial acceleration in the momentum equation. They also supposed that there is a high correlation between the radial convective velocity and the temperature fluctuations (hot fluid normally rises, cold fluid normally sinks) so that the convective heat flux can be estimated as a product of the radial velocity and the temperature perturbation. This leads to a scaling for the typical thickness ℓ of the convection columns $\ell \sim R_Q^{1/5}$, where R_Q is the flux Rayleigh number (Cardin & Olson 1994; Aubert *et al.* 2001), as described in §3 below. The 1/5 scaling law was also suggested by Ingersoll & Pollard (1982) in a discussion of convection in Jupiter’s atmosphere. The flux Rayleigh number is essentially a product of the traditional Rayleigh number and $Nu - 1$, where Nu is the Nusselt number. The inertial scaling of Aubert *et al.* is therefore not a complete prescription of the typical values achieved by nonlinear convection, but has to be supplemented by a Nusselt number–Rayleigh number relation; Aubert *et al.* used an experimentally derived power-law approximation. This is discussed further below.

Numerical simulations of fully three-dimensional convection in a sphere were pioneered by Gilman (1977, 1978), with more recent calculations from Tilgner & Busse (1997), Christensen (2001, 2002) and Aurnou & Heimpel (2004). These simulations give much useful information on the heat transport and particularly the zonal flow, but they are limited to Ekman numbers in the range 10^{-3} – 10^{-5} , because of computational expense. This is larger than the experimental values, and much larger than the typical values in planetary cores or giant-planet atmospheres. Here we report the results of quasi-geostrophic two-dimensional calculations, which can reach significantly lower Ekman numbers. The quasi-geostrophic approximation for spherical convection, QGA, was developed from the Busse (1970) annulus model by Busse (1986), Busse & Or (1986), Cardin & Olson (1994), and is described in Aubert *et al.* (2003). Yano (1992) showed that this approximation incorporates phase mixing, and Jones *et al.* (2000) showed that the quasi-geostrophic approximation gives

qualitatively reasonable results for the linear theory (see also Cole 2004). Brummell & Hart (1993) and Jones, Rotvig & Abdulrahman (2003) used the annulus model to investigate zonal flows in very rapidly rotating systems.

The aim of this paper is to investigate the different regimes of rapidly rotating convection within the QGA framework. In §2 we discuss the strengths and weaknesses of the QGA, examining the actual z -dependence of the flow at onset using the Roberts–Busse equation of linear theory. We then focus on weakly nonlinear results in §3, and investigate how far this can be extended into the strongly nonlinear regime. In §4 we compare our results with the inertial scaling laws, and also with a viscous scaling. We propose an extension of the scalings derived from the temperature equation to close the system, and investigate the nature of the boundary layers that occur at large Rayleigh number.

2. The quasi-geostrophic approximation

We use cylindrical polar coordinates (s, ϕ, z) to describe our Boussinesq convection. The case we consider in some detail is where there is differential heating, the inner core being maintained at a higher temperature than the outer sphere, but with no internal heating. The experiments closely resemble the differential heating case, but for comparison we sometimes refer to the internally heated case (see e.g. Dormy *et al.* 2004). The static temperature gradient for differential heating is

$$T_s(r) = \frac{r_i r_o (T_i - T_o)}{r_o - r_i} r^{-1} + \frac{r_o T_o - r_i T_i}{r_o - r_i} \tag{2.1}$$

where $r = \sqrt{s^2 + z^2}$, r_i is the inner core radius and r_o is the outer core radius, and T_i and T_o are the temperatures on the inner and outer boundaries. The temperature anomaly θ is defined by

$$T = T_s + \theta. \tag{2.2}$$

The radius ratio of the containing boundaries is $\eta = r_i/r_o$, the gravity field is $-g\mathbf{r}$ and the angular velocity of rotation is $\Omega\hat{\mathbf{z}}$.

The unit of length is the gap width $d = r_o - r_i$, the unit of time is d^2/κ , the thermal time, and the unit of temperature is $\Delta T = T_i - T_o$. From now on all quantities are taken to be in the dimensionless units, so $r_o = 1/(1 - \eta)$ and $r_i = \eta/(1 - \eta)$. The momentum equation is then

$$\frac{1}{P} \left(\frac{\partial \mathbf{u}}{\partial t} + \mathbf{u} \cdot \nabla \mathbf{u} \right) + 2E^{-1} \hat{\mathbf{z}} \times \mathbf{u} = -\nabla p + R\theta\mathbf{r} + \nabla^2 \mathbf{u}, \tag{2.3}$$

and the temperature and continuity equations are

$$\frac{\partial \theta}{\partial t} + (\mathbf{u} \cdot \nabla)\theta = Q(\mathbf{r})\mathbf{u} \cdot \mathbf{r} + \nabla^2 \theta \tag{2.4}$$

where $Q = \eta/((1 - \eta)^2 r^3)$ (Dormy *et al.* 2004). Incompressibility gives

$$\nabla \cdot \mathbf{u} = 0. \tag{2.5}$$

The dimensionless parameters are the Ekman number E , the Rayleigh number R and the Prandtl number P defined by

$$E = \frac{\nu}{\Omega d^2}, \quad R = \frac{g\alpha \Delta T d^4}{\kappa \nu}, \quad P = \frac{\nu}{\kappa}. \tag{2.6}$$

Using cylindrical coordinates, $\hat{\mathbf{z}} \cdot \nabla \times (2.3)$ gives

$$\frac{1}{P} \left[\frac{\partial \zeta}{\partial t} + \mathbf{u} \cdot \nabla \zeta - \boldsymbol{\omega} \cdot \nabla u_z \right] - \nabla^2 \zeta - 2E^{-1} \frac{\partial u_z}{\partial z} = -R \frac{\partial \theta}{\partial \phi}, \quad (2.7)$$

where u_z is the z -component of the velocity, $\boldsymbol{\omega} = \nabla \times \mathbf{u}$ and ζ is the z -component of the vorticity. Then $\hat{\mathbf{z}} \cdot \nabla \times (\nabla \times (2.3))$ gives

$$2 \frac{\partial \zeta}{\partial z} = E \nabla^4 u_z - \frac{E}{P} \left[\frac{\partial}{\partial t} \nabla^2 u_z + \hat{\mathbf{z}} \cdot \nabla \times \nabla \times (\mathbf{u} \times \boldsymbol{\omega}) \right] + ER \left[z \nabla_H^2 \theta - \frac{1}{s} \frac{\partial}{\partial s} \left(s^2 \frac{\partial \theta}{\partial z} \right) \right], \quad (2.8)$$

where

$$\nabla_H^2 \equiv \frac{1}{s} \frac{\partial}{\partial s} \left(s \frac{\partial}{\partial s} \right) + \frac{1}{s^2} \frac{\partial^2}{\partial \phi^2}. \quad (2.9)$$

The temperature equation is

$$\left(\frac{\partial}{\partial t} - \nabla^2 \right) \theta = Q(su_s + zu_z) - \nabla \cdot (\mathbf{u}\theta). \quad (2.10)$$

The boundary conditions are that the velocity is zero at the inner and outer boundaries and that the temperature anomaly θ vanishes there also.

The quasi-geostrophic approximation (QGA) (Aubert *et al.* 2003; Busse & Or 1986; Yano 1992) reduces this three-dimensional system to a two-dimensional system. The idea is to take advantage of the relatively weak z -dependence induced by the rapid rotation. The same philosophy has been used successfully in annulus models of rapidly rotating convection (Busse 1970). Since there is some z -dependence even in the linear problem, the QGA cannot be rigorously justified in a sphere in any limit, though it can be justified in cases where the slope of the boundary is small, as in the annulus model (not of course true for a sphere). The QGA is therefore only a model of convection in a rapidly rotating sphere. However, in cases where comparison is possible the QGA has been shown to give qualitatively correct behaviour, and it incorporates key features such as phase mixing (Yano 1992; Cole 2004; Morin & Dormy 2004).

In equation (2.8), the QGA ignores all terms on the right-hand side to give

$$\frac{\partial \zeta}{\partial z} = 0. \quad (2.11)$$

This is the essence of the QGA in rotating convection, and it is a huge simplification because the vorticity equation is reduced from three to two dimensions. Because it cannot be rigorously justified in any asymptotic limit, it is essentially a numerical approximation.

In the linear theory of convection at small E (Busse 1970; Jones *et al.* 2000), convection occurs in tall thin columns, so the horizontal derivatives are much larger, by $O(E^{-1/3})$, than the vertical derivatives. In consequence, even though E is small, only the nonlinear term and the term involving the z -derivative of θ are ignored in (2.8) in the $E \rightarrow 0$ linear theory of Jones *et al.* (2000).

In figure 1(a) we plot the z -vorticity ζ obtained from the asymptotic small- E linear theory of Jones *et al.* (2000) and Dormy *et al.* (2004) as the z -coordinate varies along the column from $z = -H$ to $z = H$. At a particular s and t , the vorticity is the real part of $\zeta \exp(im\phi)$, m being the azimuthal wavenumber that minimizes the critical Rayleigh number. The z -dependence is obtained by solving the Roberts–Busse equation (equation (3.5) of Jones *et al.* (2000) and equation (3.11) of Dormy *et al.*

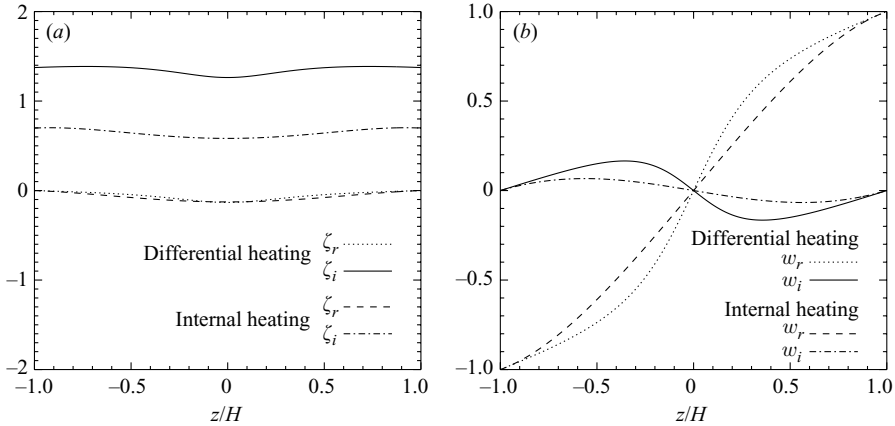


FIGURE 1. z -profiles using linear theory with $P = 1$, $\eta = 0.35$: (a) real and imaginary parts of the vorticity; (b) real and imaginary parts of the z -component of velocity.

(2004)) and is shown in two cases, both at Prandtl number $P = 1$, $\eta = 0.35$. The first case shows the real part and imaginary part of $\zeta(z) = \zeta_r + i\zeta_i$ in the case of differential heating with an inner core of radius ratio $\eta = 0.35$. In this case the critical column is located close to $s = r_i$. The second case is for uniform internal heating (for details see Dormy *et al.* 2004) where convection first onsets at $s = 0.59/(1 - \eta)$. In figure 1(b), following Aubert (2001), the real and imaginary parts of $u_z = w_r + iw_i$ are shown for the same two cases. The normalization is such that u_z is real near $z = \pm H$, and note that ζ is mainly imaginary, so that the vertical vorticity and vertical velocity are not generally in phase. Although $\zeta(z)$ is not exactly constant, the variation in z is comparatively small in both cases. The real part is also small, indicating that the column is indeed roughly parallel to the z -axis. The QGA is based on it being reasonable to ignore this small variation in ζ in the z -direction. In figure 1(a), we have only considered cases where the convection occurs outside the tangent cylinder. From now on we focus on convection outside the tangent cylinder, in the region $r_i \leq s \leq r_o$, as convection inside the tangent cylinder has a somewhat different character. Note that in the Grenoble rotating convection experiment there is only flow outside the tangent cylinder. The term $ERz\nabla_{\theta}^2\theta$ comes from the z -component of gravity, and although it is present at leading order for small E in the spherical linear theory, its neglect can be justified in experiments where gravity is replaced by centrifugal acceleration. However, the remaining terms will ensure that there is some small z -variation of ζ even in the case where the effective gravity is in the s -direction.

The arguments for the QGA above all rest on analysis of the linear modes. In nonlinear convection we expect that modes with horizontal wavelengths of order of the gap size will be excited by nonlinear interactions. However, as pointed out by Zhang & Liao (2004), any mode of this type with significant z -dependent vorticity has high frequency, $O(E^{-1})$, as the dominant term on the right-hand side of (2.8) is then the second term. Such modes are unlikely to interact much with the lower frequency $O(E^{-2/3})$ modes driven by the convection. Further justification for the QGA is provided by the experimental results. Carrigan & Busse (1983), Cardin & Olson (1994) and Aubert *et al.* (2001) all found a vertical structure that was only weakly z -dependent using visualization techniques. In summary, there will be some variation in ζ along the z -direction, but the simplification to two-dimensionality is so great that we ignore z -variations of vorticity in most of the discussion below. The

Ekman boundary layers, where there is strong z -variation of vertical vorticity, are treated by asymptotic methods.

Next we examine the relation between ζ and \mathbf{u} . In the QGA we need to assume that u_s and u_ϕ are both independent of z . When we take the z -average of (2.7), the nonlinear advection terms involve the z -averages of u_s and u_ϕ because ζ is assumed z -independent. The z -average of the term $2E^{-1}\partial u_z/\partial z$ involves u_z at the outer boundary, and through the vanishing of the radial velocity there

$$u_z|_{\pm H} = \mp \frac{su_s}{H}, \quad \text{where} \quad H(s) = \sqrt{r_o^2 - s^2}. \quad (2.12)$$

It follows that the value of u_s at the outer boundary enters the z -averaged equation (2.7) and if u_s varies along z this will in general be different from the z -averaged u_s . For tall thin columnar modes, there is no difficulty, because from (2.12) u_z is of the same order of magnitude as u_s , and if the horizontal length scales are much smaller than the vertical length scale

$$\frac{\partial u_z}{\partial z} \ll \frac{\partial u_s}{\partial s} \sim \frac{1}{s} \frac{\partial u_\phi}{\partial \phi}. \quad (2.13)$$

It then follows from $\nabla \cdot \mathbf{u} = 0$ that there is a streamfunction ψ with

$$u_\phi = -\frac{\partial \psi}{\partial s}, \quad u_s = \frac{1}{s} \frac{\partial \psi}{\partial \phi}, \quad \nabla_H^2 \psi = -\zeta, \quad (2.14)$$

so the z -independence of u_s and u_ϕ is guaranteed. For the nonlinearly excited modes with $O(1)$ horizontal wavelengths, we can again appeal to (2.7), which indicates that modes with significant z -variation in u_z and $O(1)$ horizontal length scales will have high frequencies with $\partial/\partial t \sim O(E^{-1})$, and so will not couple effectively with the columnar convection modes.

Schaeffer & Cardin (2005) give an alternative way of justifying the z -independence of u_s and u_ϕ . They do not assume $\partial u_z/\partial z$ is negligible, but instead assume u_z is a linear function of z . Figure 1(b) provides some justification for this assumption. Although $\partial u_z/\partial z$ decreases somewhat near the outer boundary, u_z is approximately linear over a large part of the columnar cells. With this linear assumption, (2.12) implies

$$u_z = -\frac{szu_s}{H^2}, \quad \text{so} \quad \frac{1}{s} \frac{\partial}{\partial s}(su_s) + \frac{1}{s} \frac{\partial u_\phi}{\partial \phi} - \frac{su_s}{H^2} = 0, \quad (2.15)$$

leading to

$$u_s = \frac{1}{s} \frac{\partial \psi}{\partial \phi}, \quad u_\phi = -\frac{\partial \psi}{\partial s} + \frac{s\psi}{H^2}, \quad \zeta = -\nabla_H^2 \psi + \frac{1}{s} \frac{\partial}{\partial s} \left(\frac{s^2 \psi}{H^2} \right). \quad (2.16)$$

Again we can deduce that u_ϕ and u_s are both individually independent of z . For short horizontal length scales, (2.16) and (2.14) are the same because the extra terms are negligible. In our numerical work we used (2.14), though some runs using (2.16) were done. For our convection problem no significant differences were found using the Cardin & Schaeffer formulation except that the Nusselt number becomes weakly s -dependent, and from now on we adopt the simpler (2.14) rather than (2.16).

We now turn to the nonlinear terms in (2.7). The term $\boldsymbol{\omega} \cdot \nabla u_z$ is negligible provided the Rossby number $Ro = |\mathbf{u}|/\Omega d$, is small everywhere, i.e. the convective vorticity is small compared to the planetary vorticity (or in experiments the rotation rate of the apparatus). This is certainly true in the experiments, and in many of the planetary applications, so this term is ignored in the QGA. We now take the z -average of (2.7)

by integrating from $z = \pm H$, where $H = \sqrt{r_o^2 - s^2}$. Following the discussion above, we replace the averaged advection term by the scalar product of the averaged \mathbf{u}_H and $\nabla\zeta$. If no-slip boundaries are present (as in all experiments) the z -derivatives of the viscous term are negligible everywhere except in the viscous boundary layer, where they give rise to an ‘Ekman pumping’ term. We use the usual Ekman layer theory, see Greenspan (1968) and Gubbins & Roberts (1987) (but note there is a sign error in their formula). We take the z -integration of (2.7) to just outside the boundary layer, where there is an ‘Ekman pumping’ normal component of velocity of order $E^{1/2}$,

$$\frac{1}{P} \left[\frac{\partial\zeta}{\partial t} + \mathbf{u} \cdot \nabla\zeta \right] + \frac{2su_s}{E(r_o^2 - s^2)} = \frac{2r_o}{E(r_o^2 - s^2)} \mathbf{u} \cdot \hat{\mathbf{n}}|_{z=H} + \nabla_H^2 \zeta - R \frac{\partial\theta}{\partial\phi}, \quad (2.17)$$

where the Ekman pumping is given by

$$\begin{aligned} \mathbf{u} \cdot \hat{\mathbf{n}}|_{z=H} &= -\frac{1}{2} E^{1/2} \hat{\mathbf{n}} \cdot \nabla \times \left[\frac{1}{(\hat{\mathbf{n}} \cdot \hat{\mathbf{z}})^{1/2}} (\hat{\mathbf{n}} \times \mathbf{u} + \mathbf{u}) \right] \\ &= -\frac{1}{2} E^{1/2} \left(\frac{H}{r_o} \right)^{1/2} \left[\zeta + \frac{su_\phi}{2H^2} - \frac{s}{H^2} \frac{\partial u_s}{\partial\phi} + \frac{5r_o}{2H^3} su_s \right]. \end{aligned} \quad (2.18)$$

Note that in deriving (2.18) we have assumed u_z is linear in z . The effect of the Ekman pumping term has been investigated recently in the annulus model by Jones *et al.* (2003). It is interesting to compare the relative importance of the first two terms on the right-hand side of (2.17). Columnar convection near onset has horizontal length scale $E^{-1/3}$ and so the internal viscous friction dominates over the Ekman pumping (Zhang & Jones 1993). For the large-scale modes such as the zonal flow this not necessarily the case, and Ekman pumping may dominate the bulk dissipation.

It is convenient to write the axisymmetric ϕ component of (2.3) in terms of the mean azimuthal velocity, the zonal flow, and this also ensures that there is no mean azimuthal pressure gradient (Plaut & Busse 2002). Denoting the average over ϕ by an overbar,

$$\left(\frac{1}{P} \frac{\partial}{\partial t} - \nabla_H^2 + \frac{E^{-1/2} r_o^{1/2}}{H^{3/2}} \right) \bar{u}_\phi = -\frac{1}{P} \overline{\mathbf{u} \cdot \nabla u_\phi}. \quad (2.19)$$

The Coriolis term is zero if u_s is z -independent, because then there can be no zonal average of u_s . If, however, there is z -dependence of u_s arising from the θ terms in (2.8), this is no longer the case and a thermal wind ensues. In the QGA we assume ζ , and hence u_s , is z -independent and so we must ignore any thermal wind. In the Grenoble experiment, the thermal wind is known to be small. The zonal flow is then entirely driven by the Reynolds stress term on the right of (2.19) which only involves the non-axisymmetric fluctuating parts of the convection. It is damped both by the Ekman pumping at the boundary and the bulk dissipation in the interior.

The temperature equation in the QGA is found by taking the z -average of (2.4) and defining

$$\langle\theta\rangle_z = \frac{1}{2H} \int_{-H}^H \theta \, dz \quad \text{and} \quad \langle T_s \rangle_z = \frac{1}{2H} \int_{-H}^H T_s \, dz. \quad (2.20)$$

We obtain, assuming $\nabla^2 T_s = 0$,

$$\left(\frac{\partial}{\partial t} - \nabla_H^2 \right) \langle\theta\rangle_z + u_s \frac{\partial \langle T_s \rangle_z}{\partial s} + \mathbf{u}_H \cdot \nabla \langle\theta\rangle_z = -\frac{1}{2H} \int_{-H}^H u_z \frac{\partial}{\partial z} (\theta + T_s) + \frac{\partial^2 \theta}{\partial z^2} \, dz. \quad (2.21)$$

The QGA temperature equation (Aubert *et al.* 2003) is obtained by omitting the terms on the right-hand side of (2.21). This is plausible, since the z -derivatives of θ will generally be smaller than the s - and ϕ -derivatives outside of thermal boundary layers, because of the columnar structure. However, it is not easy to justify rigorously, because u_z is of the same order as u_s , so the omitted term $u_z \partial T_s / \partial z$ is of the same order as the retained term $u_s \partial \langle T_s \rangle_z / \partial s$. Some insight into the nature of this approximation can be gained by considering the heat flux.

From the time-averaged (2.4) (i.e. omitting the $\partial/\partial t$ term), and integrating over $r_i \leq s' \leq s$, $-H \leq z \leq H$, $0 \leq \phi \leq 2\pi$ gives

$$\begin{aligned} \int_0^{2\pi} \int_{-H}^H \left(u_s - \frac{\partial}{\partial s} \right) (T_s + \theta) s \, dz \, d\phi - \int_{S_z} (\hat{\mathbf{n}} \cdot \nabla) (T_s + \theta) \, dS \\ = \int_0^{2\pi} \int_{-H_i}^{H_i} - \frac{\partial}{\partial s} (T_s + \theta)|_{s=r_i} r_i \, dz \, d\phi = F_t \end{aligned} \quad (2.22)$$

where F_t is the time-averaged heat flux passing through the tangent cylinder $s = r_i$, and S_z is the surface area of the ‘endcaps’ region of the outer sphere lying between $s = r_i$ and s . The first term is the convected and conducted heat flux through a cylinder of radius s , and the second term is the conducted heat flux through the endcap regions. If the QGA temperature equation

$$\left(\frac{\partial}{\partial t} - \nabla_H^2 \right) \langle \theta \rangle_z + u_s \frac{\partial \langle T_s \rangle_z}{\partial s} + \mathbf{u}_H \cdot \nabla \langle \theta \rangle_z = 0 \quad (2.23)$$

held exactly, then integrating the time-averaged (2.23) over the surface $r_i \leq s' \leq s$, $0 \leq \phi \leq 2\pi$ gives

$$\int_0^{2\pi} \left(u_s - \frac{\partial}{\partial s} \right) (\langle T_s \rangle_z + \langle \theta \rangle_z) s \, d\phi = \int_0^{2\pi} - \frac{\partial}{\partial s} (\langle T_s \rangle_z + \langle \theta \rangle_z)|_{s=r_i} r_i \, d\phi = \frac{F_t}{2H_i} \quad (2.24)$$

using (2.20) and (2.22). Now the exact convected and conducted flux through the cylinder of radius s is

$$\int_0^{2\pi} \int_{-H}^H \left(u_s - \frac{\partial}{\partial s} \right) (T_s + \theta) s \, dz \, d\phi = 2H \int_0^{2\pi} \left(u_s - \frac{\partial}{\partial s} \right) (\langle T_s \rangle_z + \langle \theta \rangle_z) s \, d\phi = \frac{H F_t}{H_i} \quad (2.25)$$

using (2.20), (2.22), and (2.24). We see that in the QGA the actual heat flux at all Rayleigh numbers passing through the cylinder at radius s of height H is just $H F_t / H_i$, and so the heat passing through the endcap regions is $(H_i - H) F_t / H_i$. The QGA thus gives a specific latitudinal distribution of heat flux through the outer sphere outside the tangent cylinder. Without a fully three-dimensional calculation or an experiment we cannot tell if this agrees with the actual latitudinal heat flux distribution, but the QGA distribution is at least plausible.

The value of $\langle T_s \rangle_z$ is the z -average of (2.1). Aubert *et al.* (2003) noted that for $\eta = 4/11 = 0.364$, the value used in all our subsequent numerical calculations, the form of the z -average of (2.1) is very close to the solution of $\nabla_H^2 \langle T_s \rangle_z = 0$ multiplied by a factor $\gamma = 0.453$, so we take (dropping the $\langle \rangle_z$ from now on)

$$T_s = T_o + \gamma \frac{\ln r_o - \ln s}{\ln r_o - \ln r_i} \quad \text{so} \quad Q = - \frac{1}{s} \frac{dT_s}{ds} = \frac{\gamma}{s^2 \ln(1/\eta)}, \quad (2.26)$$

and the temperature equation becomes

$$\frac{\partial \theta}{\partial t} + \mathbf{u}_H \cdot \nabla \theta = Q \frac{\partial \psi}{\partial \phi} + \nabla_H^2 \theta. \tag{2.27}$$

Note that if the effective gravity comes from centrifugal force as in the experiments, we need to reverse the sign of the temperature throughout, so in (2.17) the temperature term becomes $+R\partial\theta/\partial\phi$ and in (2.27) the Q term becomes $-Q(s)\partial\psi/\partial\phi$. The nature of the solution is unaffected by this transformation.

The boundary conditions adopted are that the velocity and the temperature anomaly vanish at the tangent cylinder $s = r_i$ and also at $s = r_o$, so

$$\psi = \frac{\partial \psi}{\partial s} = \theta = 0 \quad \text{at} \quad s = r_i, \quad s = r_o. \tag{2.28}$$

This boundary condition at the tangent cylinder is clearly appropriate for the Grenoble experiment configuration. The definition of the Nusselt number is quite straightforward within the QGA. The heat flux at the inner core cylinder is entirely by conduction, so

$$Nu = \frac{d\bar{T}}{ds} \left(\frac{dT_s}{ds} \right)^{-1} \quad \text{evaluated at} \quad s = r_i, \tag{2.29}$$

where \bar{T} is the azimuthal average of the temperature, gives the ratio of the total heat flux to the conducted heat flux in the basic state. It follows that

$$Nu - 1 = - \frac{\partial \bar{\theta}}{\partial s} \frac{r_i \ln(1/\eta)}{\gamma} \quad \text{evaluated at} \quad s = r_i. \tag{2.30}$$

When the inner core is a sphere, the situation is more complex. The issue of what fraction of the heat flux crosses the tangent cylinder rather than emerging from the endcaps inside the tangent cylinder lies outside the QGA framework.

We solve (2.14), (2.17) and (2.27) with boundary conditions (2.28) using a numerical scheme based on a truncated Fourier expansion in the ϕ -direction and finite differences in the s -direction, described in Aubert *et al.* (2003). The only important difference is that in this work the Ekman pumping term is included for both the non-axisymmetric and the axisymmetric components of the flow, while in Aubert *et al.* (2003) it was only applied to the axisymmetric components. The Crank–Nicolson scheme is used for all linear terms except the buoyancy term, with an explicit Adams–Bashforth scheme for the remaining terms. As the problem is only two-dimensional, a large number of grid points (typically 400) and many modes (m up to 200) can be used, even if a large coverage of parameter space is required.

3. Convection close to critical

We are considering only the convection occurring outside the tangent cylinder. We distinguish three broad regimes of convection. In order of increasing Rayleigh number these are the *weakly nonlinear* regime, the *whole-sphere* regime and the *boundary-layer* regime. At the onset of convection,

$$\psi = \Psi(s) \exp(i(m\phi - \omega_0 t)) \tag{3.1}$$

and in figure 2 we show the vorticity ζ at the onset of convection in the two cases $P = 7.0$ (water), $E = 6.5 \times 10^{-6}$ and $P = 0.025$ (gallium), $E = 1.95 \times 10^{-6}$. In the full spherical geometry convection onsets first near the tangent cylinder (Dormy *et al.*

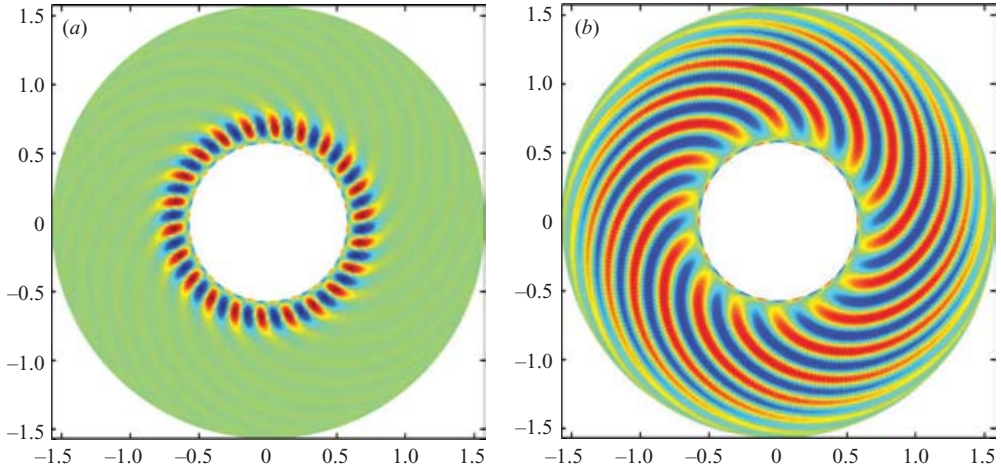


FIGURE 2. Snapshot of the vorticity in the equatorial plane at the onset of convection, viewed from above. (a) $P = 7.0$, $E = 6.5 \times 10^{-6}$, $R_c = 1.92 \times 10^7$, $m_c = 22$, $\omega_c = 1932$; (b) $P = 0.025$, $E = 1.95 \times 10^{-6}$, $R_c = 6.8 \times 10^6$, $m_c = 14$, $\omega_c = 318$.

2004), and the QGA has the same behaviour. At low Prandtl numbers, very low E is required before this localization becomes apparent (Jones *et al.* 2000), so that in practice the whole-sphere regime is entered immediately at low P . The onset value of m scales with $E^{-1/3}$ and the onset frequency with $O(E^{-2/3})$. All the main qualitative features of the linear theory with full spherical geometry are reproduced by the QGA (Aubert *et al.* 2003).

Close to critical, in the weakly nonlinear regime, the form of the convection is essentially given by the form of the linear disturbance. This regime is amenable to theoretical analysis. As the Rayleigh number is increased, the convection starts to occur over most of the sphere. This is the whole-sphere convection regime, achieved typically at Rayleigh numbers a few times critical. As the Rayleigh number is increased further, the rate of growth of Nusselt number as a function of Rayleigh number begins to slow down. We attribute this to the development of thermal boundary layers, so in this regime the heat transport is controlled by these boundary layers.

3.1. The weakly nonlinear convection regime

Near onset, for moderate or large P , in the case of differential heating, the convection is confined to a region of thickness $O(E^{2/9})$ in the s -direction (Dormy *et al.* 2004). Alternatively, the critical cylinder may be located outside the tangent cylinder, as in the whole-sphere internally heated case, in which case the convecting region is of width $O(E^{1/6})$ in the s -direction. Note that in both cases the width of the convecting region L is larger than the typical azimuthal length scale ℓ of the convection columns, which is $O(E^{1/3})$. The convection columns have a spiralling form (see figure 2(b) and Zhang 1992), and the convecting region is the envelope of these spiral columns, which may contain many different individual columns.

The behaviour near critical in the internally heated case can give rise to further complications, because the global critical Rayleigh number is larger than the local critical Rayleigh number (Jones *et al.* 2000), so there is a possibility of subcritical instability (Soward 1977). Investigations by Morin & Dormy (2004) and Cole (2004) suggested that the first bifurcation remains supercritical down to $E = 10^{-7}$, but the behaviour at very low E has yet to be fully resolved. Since this distinction between

the local and global critical Rayleigh number is lost in the differentially heated case we do not expect the complication of subcriticality in this case.

Near onset, the dynamics is dominated by the preferred single azimuthal wavenumber and the axisymmetric zonal flow, and their corresponding temperature perturbations. At larger Rayleigh numbers, nonlinear interactions ensure that the single azimuthal wavenumber broadens into a band of wavenumbers, and the axisymmetric mode is joined by a band of low-wavenumber modes. Both laboratory and numerical experiments suggest that these bands of activity do not fully merge until the Rayleigh is quite large. It is therefore helpful to write down the equations governing the interaction of a single mode with wavenumber $\exp(im\phi)$ with the axisymmetric mean flow. Let

$$\psi = \hat{\psi}(s, t) \exp(im\phi) + \text{c.c.} + \bar{\psi}(s, t), \quad \theta = \hat{\theta}(s, t) \exp(im\phi) + \text{c.c.} + \bar{\theta}(s, t). \quad (3.2)$$

The equations for the fluctuating parts neglecting the Ekman pumping are then, from (2.14), (2.17) and (2.27),

$$\hat{\zeta} + \nabla_H^2 \hat{\psi} = 0, \quad \nabla_H^2 = \left(\frac{1}{s} \frac{\partial}{\partial s} \left(s \frac{\partial}{\partial s} \right) - \frac{m^2}{s^2} \right), \quad (3.3)$$

$$\nabla_H^2 \hat{\zeta} - \frac{2im}{E(r_o^2 - s^2)} \hat{\psi} - imR\hat{\theta} = \frac{1}{P} \frac{\partial \hat{\zeta}}{\partial t} + \frac{im}{Ps} \left[\frac{\partial}{\partial s} \left(\frac{1}{s} \frac{\partial}{\partial s} (s\bar{u}_\phi) \right) \hat{\psi} + \bar{u}_\phi \hat{\zeta} \right], \quad (3.4)$$

$$\left(\frac{\partial}{\partial t} - \nabla_H^2 \right) \hat{\theta} - im \left(Q - \frac{1}{s} \frac{\partial \bar{\theta}}{\partial s} \right) \hat{\psi} = -\frac{im}{s} \bar{u}_\phi \hat{\theta}, \quad (3.5)$$

and for the mean parts, \bar{u}_ϕ being the ϕ -average of the zonal wind u_ϕ and $\bar{\theta}$ being the ϕ -average of the temperature anomaly, and complex conjugate is denoted by $*$,

$$\left[\frac{\partial}{\partial t} - \frac{1}{s} \frac{\partial}{\partial s} \left(s \frac{\partial}{\partial s} \right) \right] \bar{\theta} + \frac{im}{s} \frac{\partial}{\partial s} (\hat{\psi} \hat{\theta}^* - \hat{\psi}^* \hat{\theta}) = 0, \quad (3.6)$$

$$\frac{1}{P} \frac{\partial \bar{u}_\phi}{\partial t} - \frac{\partial}{\partial s} \left(\frac{1}{s} \frac{\partial}{\partial s} (s\bar{u}_\phi) \right) = \frac{im}{P} \frac{1}{s^2} \frac{\partial}{\partial s} \left[s \left(\hat{\psi} \frac{\partial \hat{\psi}^*}{\partial s} - \hat{\psi}^* \frac{\partial \hat{\psi}}{\partial s} \right) \right] - \frac{E^{-1/2}}{H} \sqrt{\frac{r_o}{H}} \bar{u}_\phi. \quad (3.7)$$

These equations have been integrated numerically (Cole 2004; Morin & Dormy 2004) but here we seek solutions in which the fluctuating parts have the form of travelling waves,

$$\psi = \hat{\psi}(s) \exp(i(m\phi - \omega t)) + \text{c.c.}, \quad \theta = \hat{\theta}(s) \exp(i(m\phi - \omega t)) + \text{c.c.} \quad (3.8)$$

where the t dependence has been taken out of $\hat{\psi}$ and $\hat{\theta}$, and the frequency ω is in general different from the linear frequency ω_0 , and the mean (barred) quantities are steady. Then integrating equation (3.6) we obtain

$$\frac{d\bar{\theta}}{ds} = \frac{im}{s} (\hat{\psi} \hat{\theta}^* - \hat{\psi}^* \hat{\theta}) - (Nu - 1)Qs, \quad (3.9)$$

and integrating again and using (2.26)

$$(Nu - 1)\gamma = \int_{r_i}^{r_o} \frac{im}{s} (\hat{\psi} \hat{\theta}^* - \hat{\psi}^* \hat{\theta}) ds. \quad (3.10)$$

We now take the limit $P \rightarrow \infty$. This greatly simplifies the analysis, though the method below can be used for all P . In this limit $\bar{u}_\phi \rightarrow 0$ and so all terms on the right-hand side of equations (3.4)–(3.5) disappear, and (3.7) becomes redundant. The adjoint

linear problem has solutions of the form

$$\psi = \hat{\psi}_a(s) \exp(-i(m\phi - \omega_0 t)), \quad \theta = \hat{\theta}_a(s) \exp(-i(m\phi - \omega_0 t)), \quad (3.11)$$

with

$$\hat{\zeta}_a + \nabla_H^2 \hat{\psi}_a = 0, \quad \nabla_H^2 \hat{\zeta}_a - \frac{2im}{E(r_o^2 - s^2)} \hat{\psi}_a - imQ\hat{\theta}_a = 0, \quad (3.12a, b)$$

$$i\omega_0 \hat{\theta}_a + \nabla_H^2 \hat{\theta}_a + imR_c \hat{\psi}_a = 0, \quad \hat{\psi}_a = \frac{\partial \hat{\psi}_a}{\partial s} = \hat{\theta}_a = 0 \quad \text{on } s = r_i, r_o. \quad (3.12c, d)$$

We now multiply (3.3) by $\hat{\zeta}_a$, (3.4) by $\hat{\psi}_a$, (3.5) by $\hat{\theta}_a$, add the parts together, and integrate from $s = r_i$ to $s = r_o$. Integration by parts, together with the boundary conditions (2.28) and (3.12d), gives

$$\int_{r_i}^{r_o} \left\{ -im(R - R_c) \hat{\theta} \hat{\psi}_a + i(\omega_0 - \omega) \hat{\theta} \hat{\theta}_a + \frac{im}{s} \frac{d\bar{\theta}}{ds} \hat{\psi} \hat{\theta}_a \right\} s ds = 0. \quad (3.13)$$

A useful result, easily obtained by multiplying (3.4) by $\hat{\psi}_a$, multiplying (3.12b) by $\hat{\psi}$ and subtracting and integrating, is

$$\int_{r_i}^{r_o} R \hat{\theta} \hat{\psi}_a s ds = \int_{r_i}^{r_o} Q \hat{\psi} \hat{\theta}_a s ds. \quad (3.14)$$

Using (3.9), (3.10) and (3.14), (3.13) becomes

$$\int_{r_i}^{r_o} \left\{ \hat{\psi} \hat{\theta}_a \left[mQ \frac{R - R_c}{R} - \frac{im^2}{s^2} \left((\hat{\psi} \hat{\theta}^* - \hat{\psi}^* \hat{\theta}) - \int_{r_i}^{r_o} (\hat{\psi} \hat{\theta}^* - \hat{\psi}^* \hat{\theta}) \frac{ds}{s \ln(1/\eta)} \right) \right] + (\omega - \omega_0) \hat{\theta} \hat{\theta}_a \right\} s ds = 0. \quad (3.15)$$

If the linear solution of (3.3)–(3.5) is inserted into this expression, the real and imaginary parts give $\omega - \omega_0$ and the amplitude of the linear solution in terms of $(R - R_c)/R$. Together with (3.10) we get an expression for the Nusselt number and frequency change in terms of the Rayleigh number,

$$Nu - 1 = K_1 \frac{R - R_c}{R}, \quad \omega - \omega_0 = K_2 \omega_0 \frac{R - R_c}{R}. \quad (3.16)$$

For $E = 2.44 \times 10^{-6}$, $\eta = 4/11$, $P = \infty$, and no Ekman pumping, the linear critical value of $R_c = 8.12 \times 10^7$, $\omega_0 = 4822$ and the critical value of $m = 34$. Both the linear problem and the adjoint problem were solved numerically, and values of $K_1 = 0.17$ and $K_2 = 0.25$ were found. In figure 3 we plot $Nu - 1$ against $R/R_c - 1$ using the fully two-dimensional QGA, at a number of values including $P = 7$, $E = 2.44 \times 10^{-6}$. The slope at low $R/R_c - 1$ of the $P = 7$ points is very close to the slope predicted by (3.16), showing that the $P \rightarrow \infty$ theory is reasonable for $P = 7$.

It is interesting to compare the results (3.16) with large-Prandtl-number non-rotating convection. For two-dimensional rolls in Bénard convection in the weakly nonlinear regime a relation of the form (3.16) holds but with $K_1 = 2$ in the stress-free case. Tilgner & Busse (1997) found $K_1 \approx 0.5$ at the much larger Ekman number of 2×10^{-3} in fully three-dimensional spherical simulations. So the rotation is substantially reducing the convective heat transport in the weakly nonlinear regime. Partly, this is due to the oscillatory nature of the convection, which means that $\hat{\theta}$ and \hat{u}_s are out of phase, whereas in non-rotating convection they are exactly in phase at onset. It is also partly due to the comparatively thin region, of $O(E^{2/9})$ (Dormy *et al.*

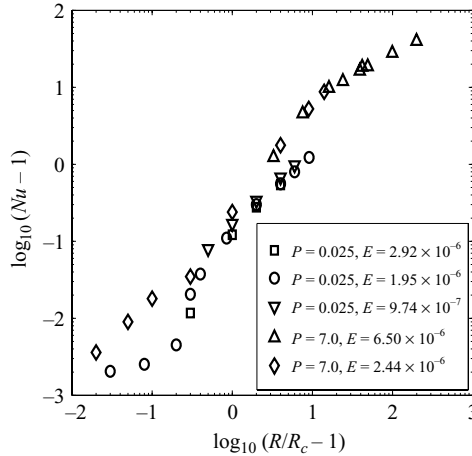


FIGURE 3. Reduced Nusselt number $Nu - 1$ as a function of R/R_c for various P and E .

2004), near the tangent cylinder where convection is significant (see figure 2a). If we suppose the thickness of this layer is L , then in (3.10) the integral will only be significant over a region of thickness L , so $Nu - 1$ scales as $L|\hat{\psi}\hat{\theta}^* - \hat{\psi}^*\hat{\theta}|$. But from (3.15), $(R - R_c)/R$ scales directly as $|\hat{\psi}\hat{\theta}^* - \hat{\psi}^*\hat{\theta}|$, so K_1 must scale linearly with L , and hence is small at very small E . There is also the possibility of relaxation oscillations (Grote & Busse 2001; Morin & Dormy 2004), even at large P (Cole 2004), where the convection occurs in bursts, with long periods of much reduced convective activity. This may account for the low Nu value at $R/R_c - 1 \approx 0.3$. The Nusselt number increases slightly faster than the (3.16) prediction near $R/R_c - 1 \approx 1$, and this may be due to convection now occurring in the whole sphere, rather than just near $s = r_i$.

The slope K_1 is also small at low P (in fact considerably smaller than at large P) but for a different reason. We can see this by looking at the $P = 0.025$ points in figure 3, where initially $Nu - 1$ only climbs slowly as $R/R_c - 1$ increases (see also Tilgner & Busse 1997). This is due to the suppression of convection by the inertial terms (Herrmann & Busse 1997; Plaut & Busse 2002). There is also very strong time-dependence at low P due to instabilities occurring close to onset (Schnaubelt & Busse 1992; Plaut & Busse 2002). However, as noted by Plaut & Busse (2002), as the Rayleigh number increases, the zonal wind changes its form and the convection restabilizes. The convection is then not so strongly impeded, and the Nusselt number starts to increase more rapidly, as seen in figure 3.

3.2. The local Péclet number

We can rewrite (3.15) in another form, eliminating the integral using (3.10),

$$\int_{r_i}^{r_o} \left\{ \hat{\psi}\hat{\theta}_a \left(mQR_c - mNuRQ + \frac{im^2R}{s^2} (\hat{\psi}\hat{\theta}^* - \hat{\psi}^*\hat{\theta}) \right) - R(\omega - \omega_0)\hat{\theta}\hat{\theta}_a \right\} s \, ds = 0. \quad (3.17)$$

To make further progress we need to obtain a relation between $R\hat{\theta}$ and $\hat{\psi}$. While these are both nonlinear quantities whose form varies strongly with R , we explore the consequences of assuming that their ratio remains fixed at its linear value,

$$R\hat{\theta} \approx (\Gamma_r + i\Gamma_i)\hat{\psi}. \quad (3.18)$$

The factor R is suggested by (3.4), and Γ varies with s in a way easily computed from linear theory. One way of viewing this approximation is that the mean temperature

gradient in the interior is reduced by a factor R_c/R through the action of the mean temperature anomaly $\bar{\theta}$ in equation (3.5) as the convection becomes more nonlinear, but apart from this factor the linear relation between $\hat{\theta}$ and $\hat{\psi}$ is maintained. We now obtain

$$\int_{r_i}^{r_o} \hat{\psi} \hat{\theta}_a \left[1 - \frac{NuR}{R_c} + \frac{2m\Gamma_i}{R_c Qs^2} |\hat{\psi}|^2 - \frac{(\omega - \omega_0)(\Gamma_r + i\Gamma_i)}{mQR_c} \right] s \, ds \approx 0. \quad (3.19)$$

If all the terms in the square brackets were constant, the imaginary part would imply that $\omega = \omega_0$. This is not of course strictly true, as K_2 in (3.16) is not exactly zero, but nevertheless the $\omega - \omega_0$ term seems to be relatively unimportant and so we obtain

$$\frac{RNu}{R_c} - 1 \approx \frac{2m\Gamma_i}{R_c Qs^2} |\hat{\psi}|^2 \approx \frac{2}{3} |\hat{\psi}|^2 \quad (3.20)$$

where the numerical approximation comes from using the local theory of convection at small E (Busse 1970; Jones *et al.* 2000), ignoring the radial wavenumbers compared to the azimuthal wavenumbers, which is valid for very small E in the case of differential heating (Dormy *et al.* 2004). This theory gives $R_c Qs^2 = 3m^4/s^4$ and $\Gamma_i = m^3/s^4$ at the critical value of m , and $s = r_i$ gives minimum critical R_c .

Since $u_s = (1/s)\partial\psi/\partial\phi$, if we define a length scale $\ell_c = 2\pi r_i/m$ where m is the critical wavenumber at onset, then

$$|\ell_c u_s| \approx 2\pi |\psi|. \quad (3.21)$$

ℓ_c is then a measure of the azimuthal length scale of the convection near onset, since convection first onsets near the tangent cylinder. In dimensional units, $|\ell_c u_s|$ is $u_s \ell_c / \kappa = Pe_\ell$, and is therefore a local Péclet number, based on the length scale of the convection, ℓ_c . With the definition (3.2), the root-mean-square time-average of $|u_s| = \hat{U}_s = (\sqrt{2}m/s)|\hat{\psi}|$ and so (3.20) predicts

$$Pe_\ell = \ell_c \hat{U}_s \approx 2\pi\sqrt{2}|\hat{\psi}| \approx 2\pi\sqrt{3}p^{1/2} = 10.9p^{1/2}, \quad \text{where } p = \frac{RNu}{R_c} - 1. \quad (3.22)$$

There are various approximations involved in (3.22), and the basic assumption that the solutions are periodic is far from true as soon as R is a few percent above critical. It is therefore quite remarkable that the plot of the local Péclet number against p for Prandtl number 7, figure 4(a), has a slope of almost exactly 0.5 over the whole range of Rayleigh numbers for which we were able to compute, up to nearly 50 times critical. Even the prefactor of 10.9 given by (3.22) is close; the best fit from a log-log regression gave

$$Pe_\ell = 8.6p^{1/2}. \quad (3.23)$$

We also include some low- P points in figure 4(a) for comparison. Our theory has only been developed for large P , so low- P points are not expected to obey (3.22). At small p , Pe_ℓ is much reduced at $P = 0.025$, consistent with the low- P behaviour in figure 3, but at larger p even the low- P points are beginning to fall close to (3.23).

The temperature fluctuation can also be predicted using (3.18). Again using (3.2) and taking the time-average, $|\theta| = \hat{\Theta}_c = \sqrt{2}|\hat{\theta}|$. We obtain using (3.20)

$$\frac{R\hat{\Theta}_c}{R_c \ell_c} = \frac{|\Gamma||\hat{\psi}|m}{\sqrt{2}\pi s R_c} \approx \frac{\gamma}{2\pi s \ln(1/\eta)} p^{1/2} \approx 0.12p^{1/2} \quad (3.24)$$

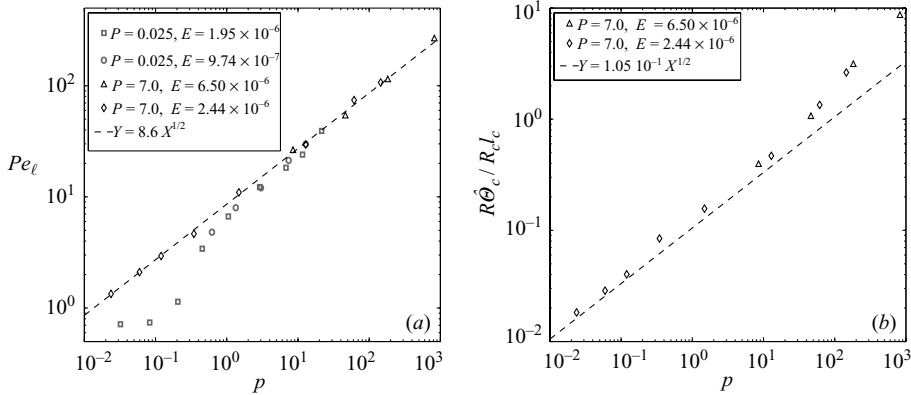


FIGURE 4. Scaling of (a) local Péclet number $Pe_\ell = \hat{U}_s \ell_c$, (b) temperature perturbation $R\hat{\Theta}_c/R_c \ell_c$, as a function of the parameter $p = RNu/R_c - 1$ for $P = 7.0$ and various E . Points are from the QGA calculations, and the dashed curves are given by (3.22) and (3.24).

where we have adopted a value of s close to the tangent cylinder. We have also used the local theory value of $\Gamma_r = \sqrt{2}m^3/s^4$. In figure 4(b), $\ln(R\hat{\Theta}_c/R_c \ell_c)$ is plotted against $\ln p$, and the dashed line $R\hat{\Theta}_c/R_c \ell_c = 0.12p^{1/2}$ is shown.

To obtain figure 4, and subsequent plots involving averaged quantities, the root-mean-square average over t and ϕ is taken, and then the maximum over s is found. Thus

$$\hat{U}_s = \max_{r_i < s < r_o} \left[\frac{1}{2\pi\tau} \int_\tau \int_0^{2\pi} |u_s(s, \phi, t)|^2 d\phi dt \right]^{1/2}, \quad (3.25)$$

and similarly to obtain the other averaged quantities. Note that the temperature fluctuation $\hat{\Theta}$ used to plot figure 4(b) is the non-axisymmetric part of the temperature only. Interestingly, although the results at moderate p are in good agreement with the predictions, at higher R (3.24) is beginning to significantly underpredict the true value of the temperature fluctuation. This is probably connected with the transition from whole-sphere convection to a boundary-layer-dominated regime. As we see later, at large R the temperature fluctuations are largest in the boundary layer, and so our method of taking the maximum over s may be contributing to the upturn in $\hat{\Theta}_c$ at large R .

4. Scaling laws for strongly nonlinear convection

4.1. The inertial scaling

An important issue for rapidly rotating convection at large R is how the various quantities scale with R , E and P . On the basis of laboratory experiments, Aubert *et al.* (2001) proposed an inertial scaling, which was also suggested by Ingersoll & Pollard (1982). The scaling is based on the idea that the length scale perpendicular to the rotation axis, ℓ , is shorter than the container length scale. At these large values of R we assume that there is no distinction between the typical length scale ℓ in the radial and azimuthal directions, and that ℓ is a dominant length scale for the convectively driven vortices. We distinguish between the typical velocity of the non-axisymmetric fluctuating convection \hat{U}_c and that of the axisymmetric zonal flow \hat{U}_ϕ^0 , which scale differently. The radial and azimuthal components of the convective velocity are assumed to be similar for our scaling, and when we compare with the

QGA results we define \hat{U}_c to be the average, as defined in (3.25), of $(u_\phi^2 + u_s^2)^{1/2}$ where u_ϕ is the non-axisymmetric part only. In the inertial scaling it is assumed that inertial and Coriolis accelerations are in balance with the buoyancy force for the non-axisymmetric components, so using (2.17)

$$\zeta \sim \frac{\hat{U}_c}{\ell}, \quad \frac{1}{P} \mathbf{u} \cdot \nabla \zeta \sim \frac{2su_s}{E(r_o^2 - s^2)} \sim R \frac{\partial \theta}{\partial \phi}, \quad (4.1a-c)$$

where only the non-axisymmetric parts of ζ and \mathbf{u} are involved, leads to

$$\frac{\hat{U}_c^2}{P\ell^2} \sim \frac{\hat{U}_c}{E} \sim \frac{R\hat{\Theta}_c}{\ell}, \quad (4.2)$$

where $\hat{\Theta}_c$ is the typical non-axisymmetric temperature fluctuation. The second assumption is that the convective heat flux scales as $\hat{U}_c\hat{\Theta}_c$, recalling that we assume that the fluctuating u_s scales with \hat{U}_c . Then

$$Nu - 1 \sim \hat{U}_c\hat{\Theta}_c. \quad (4.3)$$

This assumes the correlation between the radial velocity and the temperature fluctuation does not vary much with R , E or P . In so far as we have been able to test this numerically, (4.3) does seem reasonable. Then (4.2) and (4.3) give the scalings

$$\hat{U}_c \sim (EP)^{1/5} R_Q^{2/5}, \quad (4.4a)$$

$$R\hat{\Theta}_c \sim (EP)^{-1/5} R_Q^{3/5}, \quad (4.4b)$$

$$\ell \sim E^{3/5} P^{-2/5} R_Q^{1/5}, \quad \text{where } R_Q = R(Nu - 1). \quad (4.4c)$$

These formulae can easily be written in terms of R_Q/R_c assuming that $R_c \sim [E(1+P)/P]^{-4/3}$ (Busse 1970). The length scale ℓ is known as the Rhines scale (Rhines 1975), as it is given by the balance of Coriolis and inertial accelerations. The inertial scaling is incomplete, as it does not determine the relation between $Nu - 1$ and R . Either a further independent assumption is needed (see §4.3 below), or the Nusselt number can be determined experimentally as a function of R , as in Aubert *et al.* (2001).

For the zonal flow, we follow Aubert *et al.* (2001) and assume a balance between the Reynolds stress and the Ekman pumping,

$$\overline{(\mathbf{u} \cdot \nabla) u_\phi} = \frac{\partial}{\partial s} \overline{u_s u_\phi} \sim \frac{\hat{U}_c^2}{\ell} \sim \frac{P}{E^{1/2}} \bar{u}_\phi, \quad (4.5)$$

which gives

$$\hat{U}_\phi^0 \sim E^{3/10} P^{-1/5} R_Q^{3/5}. \quad (4.6)$$

There are two further assumptions in (4.6). The first is that the Ekman pumping is more important in damping the zonal flow than the internal friction. This appears to be true for low Prandtl numbers, but not for high Prandtl numbers, where the volume dissipation dominates the Ekman pumping (see §4.2 below). The second assumption is that the correlation between u_s and u_ϕ does not change significantly with R , E and P . This is only true near critical, and we return to this point below.

We test (4.4a) and (4.6) by plotting in figure 5(a), \hat{U}_c against $R_Q(EP)^{1/2}$, and in figure 5(b), $\hat{U}_\phi^0 P^{1/2}$ against $R_Q(EP)^{1/2}$. Note that the quantity $R_Q(EP)^{1/2}$ is independent of viscosity (as is the scaling for the convective velocities), so the inertial scaling predicts a convective velocity independent of viscosity, as expected. If the inertial scalings

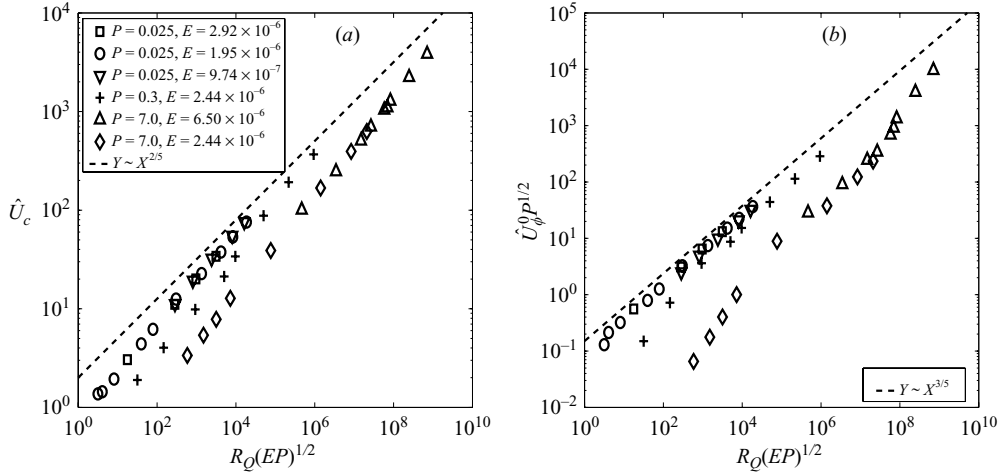


FIGURE 5. Test of the inertial scaling with our QG code, including the Ekman pumping for various E and P . (a) \hat{U}_c plotted against $R_Q(EP)^{1/2}$. (b) $\hat{U}_\phi^0 P^{1/2}$ plotted against $R_Q(EP)^{1/2}$.

held, all points in figure 5(a) should collapse onto a single line of slope $2/5$ and in figure 5(b) onto a single line of slope $3/5$. The dependence on R_Q and E fits reasonably well, but the dependence on P does not fit at all well. This is a serious problem for the inertial scaling, because the key assumption that the inertial and Coriolis terms balance is where the Prandtl-number dependence enters the scaling. There is some evidence in figure 5(a) that at the highest Rayleigh numbers the $P = 7$ results are creeping back to the $(EP)^{1/5} R_Q^{2/5}$ line, but at these very high Rayleigh numbers and only comparatively moderate Ekman numbers, convection is likely to be three-dimensional and the QGA may break down. It appears that in the regime where simulations are feasible the viscosity is still important in determining the convective velocity. In figure 5(b), the inertial scaling does reasonably well at low P , but the zonal flow at $P = 7$ is far below the value predicted by the inertial scaling. This is not so surprising, because the neglected bulk dissipation term is important in the dynamics of the zonal flow at $P = 7$.

An alternative viscous scaling is to replace (4.2) by

$$\frac{\hat{U}_c}{E} \sim \frac{R\hat{\Theta}_c}{\ell}, \quad \ell \sim \left(\frac{E(1+P)}{P} \right)^{1/3}, \quad (4.7)$$

where the length scale ℓ is determined by linear theory, $\ell = \ell_c = 2\pi r_i/m$. The P -dependence used here is that found from the annulus model (Busse 1970). At large P , ℓ becomes P independent, but at small P , $\ell \sim (E/P)^{1/3}$. This leads to

$$\hat{U}_c \sim E^{1/3} \left(\frac{P}{1+P} \right)^{1/6} R_Q^{1/2}, \quad (4.8a)$$

$$R\hat{\Theta}_c \sim E^{-1/3} \left(\frac{P}{1+P} \right)^{-1/6} R_Q^{1/2}, \quad (4.8b)$$

$$\hat{U}_\phi^0 \sim E^{5/6} P^{-1/3} R_Q, \quad (4.8c)$$

using the small- P form in (4.8c) since it will only be valid when Ekman suction dominates bulk dissipation in (2.19) which only happens at low P . The E -dependence

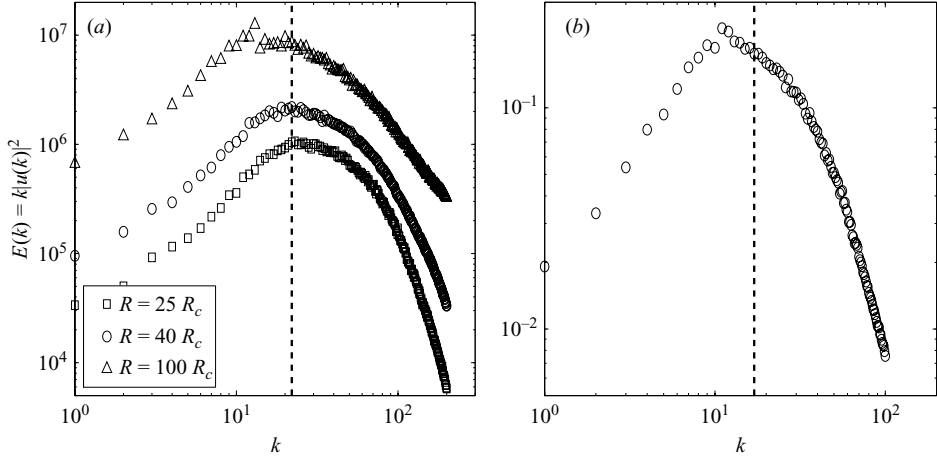


FIGURE 6. Spectrum of the kinetic energy $E(k)$ with the linear critical k marked as dashed lines. (a) $P = 7.0$, $E = 6.5 \times 10^{-6}$, $R = 25R_c$, $40R_c$ and $100R_c$; (b) $P = 0.025$, $E = 9.74 \times 10^{-7}$, $R = 3.5R_c$.

and the R_Q -dependence are very similar in both the viscous and inertial scalings. Indeed, if R_Q/R_c is kept constant, the E -dependence is the same for both scalings. Aubert *et al.* (2001) considered that a fixed ℓ fitted their experimental data better than the ℓ prescribed by (4.4c). For \hat{U}_c , the data cannot distinguish which gives the better fit as far as the E and R_Q dependence is concerned. The scatter of the P -dependence is considerably reduced if (4.8a) is used. The R_Q dependence from (4.8c) is now too steep for the data at large R . However, this may be connected with the Reynolds stress not scaling with \hat{U}_c^2/ℓ owing to progressive decorrelation of u_ϕ and u_s .

In figure 6(a) we show the energy spectrum $E(k) = k|u_c(k)|^2$ for $P = 7.0$, $E = 6.5 \times 10^{-6}$, for three values of the Rayleigh number. $E(k)$ has the dimensions L^3T^{-2} , and its integral over $0 < k < \infty$ and the convecting region is the total energy. To obtain $E(k)$ we set $k = m/r_i$, m being the azimuthal wavenumber, let

$$u_s = \frac{1}{2} \left(\sum_{m=1}^M u_s^m(s, t) \exp(im\phi) + \text{c.c.} \right) \quad (4.9)$$

and take the root-mean-square average $|u_s^m(s, t)|$ over the whole sphere and time. Doing the same for u_ϕ we set $E(k) = k\{\langle |u_s^m|^2 \rangle_{s,t} + \langle |u_\phi^m|^2 \rangle_{s,t}\}$. Figure 6(b) shows the equivalent picture for $P = 0.025$, $E = 9.74 \times 10^{-7}$, $R = 3.5R_c$. The dashed lines in figure 6 correspond to the critical value for the onset of convection. We see that at $25R_c$ and $50R_c$ there is a significant peak near k_{crit} . At the largest value, $100R_c$, the peak has shifted slightly to a lower wavenumber, but there is remarkably little evidence of an inverse cascade pushing energy to higher wavenumbers. The spectrum appears to be determined by the balance of driving and dissipation, so the arguments leading to a $k^{-5/3}$ spectrum for wavenumbers below the ‘forcing’ wavenumber (see e.g. Salmon 1998) do not apply. In figure 6(b) the peak has shifted somewhat, but surprisingly little considering that at $P = 0.025$, $R = 3.5R_c$ corresponds to a strongly turbulent regime. The persistence of the linear critical wavenumber, which is Prandtl-number dependent, even at rather large Rayleigh numbers may account for the failure of the different Prandtl-number results to collapse onto the inertial scaling line in figure 5(a).

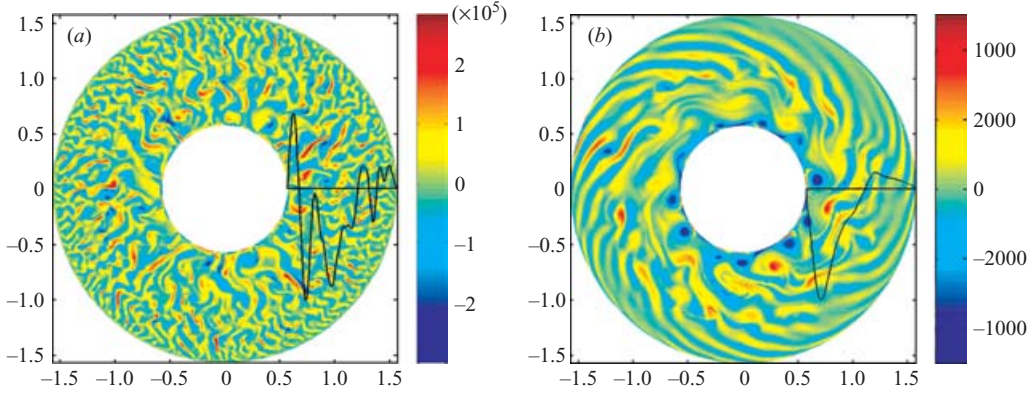


FIGURE 7. Vorticity snapshots with the zonal flow profile added. (a) $P = 7.0$, $E = 6.5 \times 10^{-6}$, $R = 42.7R_c$; (b) $P = 0.025$, $E = 1.95 \times 10^{-6}$, $R = 3.0R_c$.

In figure 7(a) we show a snapshot of the vorticity at $P = 7.0$, $E = 6.5 \times 10^{-6}$, $R = 42.7R_c$, and in figure 7(b) the vorticity for $P = 0.025$, $E = 1.95 \times 10^{-6}$, $R = 3R_c$. The highly chaotic nature of the flow is evident, as is the prevalence of the small length scale ℓ in figure 7(a), and in figure 7(b) the persistence of ‘linear’ behaviour (compare the linear theory figure 2(b) at the same P).

4.2. The zonal flow

The zonal flow profile is also shown in figures 7(a) and 7(b). The zonal flow has a consistently different pattern at large and small P . At $P = 7$, with the figure 7(a) parameter values, $\hat{U}_c \approx 1723$, $\hat{U}_\phi^0 \approx 573$, so the zonal flow is only one third of the convective velocity. At $P = 0.025$ and the figure 7(b) parameter values, $\hat{U}_c \approx 44$, $\hat{U}_\phi^0 \approx 106$, so the zonal flow is double the convective velocity. The zonal flow takes up a much larger fraction of the kinetic energy at low P . At large P , the weak zonal flow has multiple jets, whereas the stronger zonal flow has a much simpler spatial structure with strong retrograde flow near the tangent cylinder. Note also that although the convective velocity \hat{U}_c is smaller in figure 7(b) than in figure 7(a) in terms of the thermal time scale, the Reynolds number \hat{U}_c/P is much larger in figure 7(b) than in figure 7(a), despite the Rayleigh number in figure 7(b) being only three times critical.

In figures 8(a) and 8(b), the various terms involved in zonal flow production are analysed: the Ekman pumping (labelled EP), the bulk dissipation (labelled BD) and the Reynolds stress (RS). These are found by averaging the terms in (2.19) over cylinders of constant s . We see from figure 8 that at high P the bulk dissipation is mainly balancing the Reynolds stress, with Ekman pumping playing only a minor role, but at low P the Ekman pumping balances the Reynolds stress, the bulk dissipation being relatively unimportant. Rather remarkably, although the Ekman pumping makes only a small global contribution in figure 8(a), it nevertheless makes a huge difference to the pattern of the zonal flow. If the Ekman pumping is switched off, the zonal flow is much larger and multiple jets do not occur; similar behaviour was found in the annulus model (Jones *et al.* 2003; Rotvig & Jones 2005).

As mentioned above, the scaling $(\mathbf{u} \cdot \nabla) \mathbf{u}_\phi \sim \hat{U}_c^2/\ell$ suggested by weakly nonlinear theory does not fit well with our QGA data at larger R . In the weakly nonlinear regime, \hat{U}_ϕ^0 increases quadratically with \hat{U}_c , but at larger Rayleigh numbers \hat{U}_ϕ^0 grows only at a rate \hat{U}_c^x , with $1 < x < 2$. Since the zonal flow is driven by Reynolds force

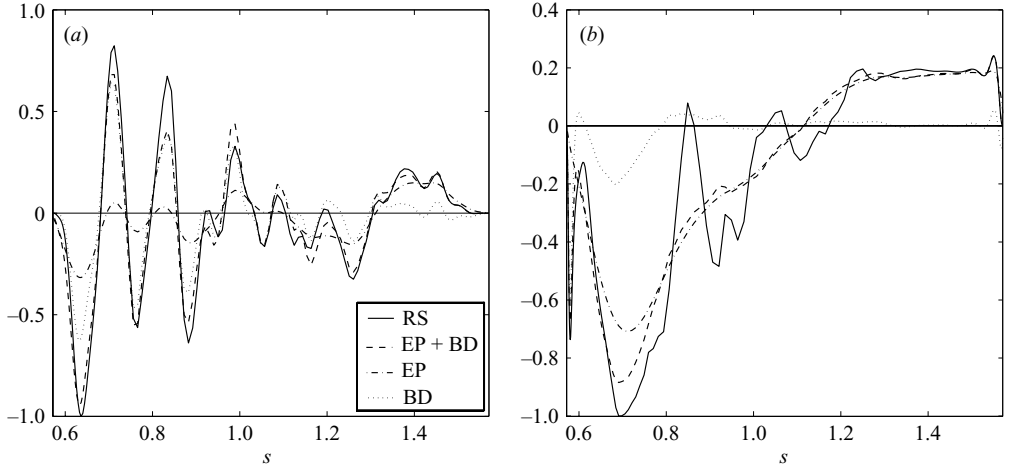


FIGURE 8. Profiles of the different terms in equation (2.19); Ekman pumping (EP), bulk dissipation (BD), Reynolds stress (RS). These s -profiles are averaged over ϕ and time. (a) $P = 7.0$, $E = 2.44 \times 10^{-6}$, $Re = 10R_c$; (b) $P = 0.025$, $E = 1.95 \times 10^{-6}$, $Re = 3.0R_c$.

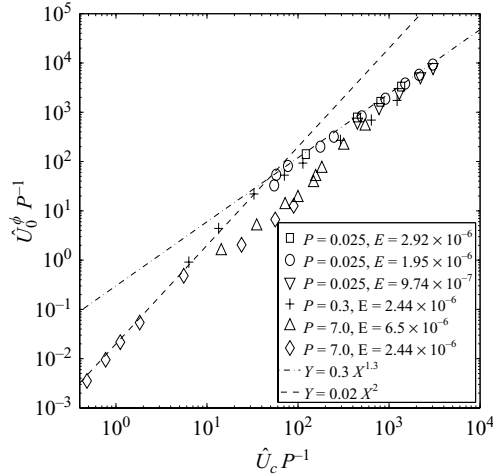


FIGURE 9. Zonal flow $P^{-1}\hat{U}_\phi^0$ as a function of convective Reynolds number $P^{-1}\hat{U}_c$. The dashed line gives the quadratic weakly nonlinear scaling, and the dot-dash line gives a power 1.3 scaling which appears to fit the low- P data.

in the QGA, we investigate the dependence of \hat{U}_ϕ^0 on \hat{U}_c . The viscous scaling (4.8a) and (4.8c) gives $\hat{U}_\phi^0 \sim E^{1/6} P^{-2/3} \hat{U}_c^2$ at low P , i.e. the weakly nonlinear quadratic dependence. The inertial scaling (4.4a) and (4.6) gives $P^{-1}\hat{U}_\phi^0 \sim (P^{-1}\hat{U}_c)^{3/2}$. Since $P^{-1}\hat{U}_c$ is the convective velocity in terms of ν/d rather than κ/d , it is a Reynolds number rather than a Péclet number, and we plot in figure 9 $P^{-1}\hat{U}_\phi^0$ against $P^{-1}\hat{U}_c$. The low- P results, where the assumption that the Reynolds force balances the Ekman pumping is valid, lie approximately on a line

$$P^{-1}\hat{U}_\phi^0 \sim 0.3(P^{-1}\hat{U}_c)^{1.3}, \quad (4.10a)$$

suggesting that at large Re the Reynolds force

$$u_s \frac{\partial u_\phi}{\partial s} \sim \frac{u_s u_\phi}{\ell} \sim \hat{U}_c^x, \quad \text{where } x \approx 1.3. \quad (4.10b)$$

There are a number of possible explanations for this behaviour. Noting that the exponent 1.3 is less than the 3/2 predicted by inertial theory, Gillet *et al.* (2006) suggest that with strong zonal flow and large Re , the radial length scale ℓ in (4.10b) may be increasing with Re as an inverse cascade eventually begins to develop. With strong zonal flow, the vorticity may be dominated by the zonal flow contribution $\partial \hat{U}_\phi^0 / \partial s$, so the Rhines balance (4.1b), $P^{-1} \mathbf{u} \cdot \nabla \zeta \sim 2su_s/E(r_o^2 - s^2)$, would lead to

$$\ell \sim (EP^{-1} \hat{U}_\phi^0)^{1/2}, \quad (4.11a)$$

so that (4.5) gives

$$\frac{\hat{U}_c^2}{\ell} \sim \frac{\hat{U}_c^2}{(EP^{-1} \hat{U}_\phi^0)^{1/2}} \sim PE^{-1/2} \hat{U}_\phi^0, \quad \text{so } P^{-1} \hat{U}_\phi^0 \sim (P^{-1} \hat{U}_c)^{4/3}, \quad (4.11b)$$

which is not far from the observed relationship. Note that if the Rhines length follows (4.11a) rather than $\ell \sim (EP^{-1} \hat{U}_c)^{1/2}$, (4.4a) and (4.4c) must be modified to

$$\hat{U}_c \sim E^{3/16} P^{1/4} R_Q^{3/8}, \quad \ell \sim E^{5/8} P^{-1/2} R_Q^{1/4}. \quad (4.11c, d)$$

Another possibility is that the reduction in the rate of growth of the Reynolds force with Re is due to a progressive decorrelation between u_s and u_ϕ , so that even if ℓ were constant, and $u_s \sim u_\phi \sim \hat{U}_c$, the Reynolds force could fall. Some evidence for this decorrelation is found by comparing figures 2(b) and 7(b).

At large P and R the primary balance in (2.19) is Reynolds stress against bulk dissipation. The trend in figure 9 for the $P = 7$ points is not very clear, but since the zonal flow is weak and from figure 6(a) there is little evidence for ℓ increasing with \hat{U}_c , it is simplest to assume the Reynolds force scales as $\hat{U}_c^{1.3}/\ell_c$, leading to

$$P \frac{\hat{U}_\phi^0}{\ell_c^2} \sim \frac{\hat{U}_c^{1.3}}{\ell_c}. \quad (4.12)$$

We can now suggest scalings for \hat{U}_ϕ^0 at larger R based on these ideas. At low P we use (4.11b) and (4.11c) and at high P we use (4.12) and (4.8a) to give

$$\hat{U}_\phi^0 \sim E^{1/4} R_Q^{0.5}, \quad P \ll 1; \quad \hat{U}_\phi^0 \sim E^{0.77} P^{-1.12} R_Q^{0.65}, \quad P \gg 1. \quad (4.13a, b)$$

These formulae fit quite well with the data in figure 5(b). There are, however, a number of issues concerning the range of validity of these formulae. There is some uncertainty about the size of the convective length scale ℓ . Here we find there is not so much variation of ℓ with R (see e.g. figure 6a), but the annulus model study of Jones *et al.* (2003) suggested that the length scale of the zonal flow increases with R_Q . Also, the correct relationship between the zonal and convective flows depends on the correlation between u_s and u_ϕ . If there is progressive decorrelation as the flow becomes more turbulent, that decorrelation needs to be taken into account in formulae such as (4.13). Another point is that in (4.13a) we assume the primary balance is between Ekman suction and Reynolds stress whenever P is small. If the zonal flow length scale does scale approximately with ℓ at low E , the bulk dissipation might start to become important at $E \ll 10^{-6}$ even at low P .

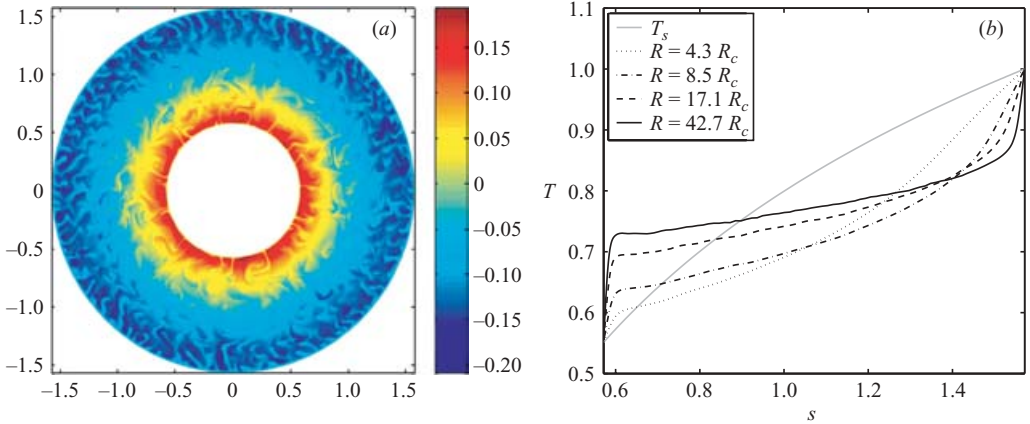


FIGURE 10. (a) Snapshot of the temperature perturbation θ at $P = 7.0$, $E = 6.5 \times 10^{-6}$, $R = 42.7 R_c$. (b) Profile of the temperature \bar{T} at varying R , for $P = 7.0$ and $E = 6.5 \times 10^{-6}$.

4.3. Heat transport at large R

We noted above that both the inertial scaling and the viscous scaling are incomplete, because the Nusselt number–Rayleigh number relation is undetermined. In figure 10(a), a snapshot of the temperature anomaly θ is shown for a strongly supercritical case at $P = 7$. Thin plumes emerging from the tangent cylinder are evident. In figure 10(b) the mean temperature profile \bar{T} averaged over ϕ and time is shown. It is clear that at large R , thin thermal boundary layers are forming, and the plumes are emerging from these layers. At low P it is hard to get into the large- Nu regime with our code, and so in this section we address only the large- P case. It should be noted that the QGA breaks down at $s = r_o$, and so the thermal boundary layer structure near $s = r_o$ may be unreliable. We therefore focus on the tangent cylinder boundary layer, and assume the Grenoble experiment configuration, where this is a solid boundary.

A natural extension to the scaling laws is

$$\overline{(\mathbf{u} \cdot \nabla) \theta} \sim u_s \frac{d\bar{T}}{ds} \quad \text{or} \quad \hat{\Theta}_c \sim \ell(\gamma - \Delta T') \quad (4.14)$$

where from (2.26) γ is the temperature drop from r_i to r_o , and $\Delta T' = \Delta T'_i + \Delta T'_o$ is the total temperature drop across both the boundary layer at the tangent cylinder and the boundary layer near the equator, so $\gamma - \Delta T'$ is the temperature drop across the convecting region. At moderate R we see from figure 10(b) that $\Delta T'$ is small, but at large R , $\Delta T'$ approaches γ .

If we use the inertial scaling (4.2), (4.3) with (4.14) we obtain

$$Nu - 1 \sim R^{3/2} P^{-1/2} E^2 (\gamma - \Delta T')^{5/2}, \quad (4.15a)$$

while the viscous scaling (4.3), (4.7) and (4.14) gives

$$Nu - 1 \sim R \left(\frac{1+P}{P} \right)^{1/3} E^{4/3} (\gamma - \Delta T')^2. \quad (4.15b)$$

Equation (4.15b) appears to fit the moderate- R data better (see figure 3). It also has the same R -dependence as the weakly nonlinear theory, and it predicts $R_Q \sim R^2$

provided $\Delta T'$ is small. At large R , $\Delta T'$ becomes significant, and Nu starts to increase more slowly than linearly with R .

We can estimate the growth of the temperature drop $\Delta T'_i$ near the tangent cylinder by using a boundary-layer argument, assuming the presence of a solid cylinder at $s = r_i$. We take the thermal boundary layer to be of thickness δ_κ and the viscous boundary layer (thicker at large P) to have thickness δ_ν . Balancing advection and diffusion across these layers,

$$\delta_\kappa^2 \sim \frac{\ell}{U^*}, \quad \delta_\nu^2 \sim \frac{\ell P}{U^*} \tag{4.16a, b}$$

where U^* is the typical velocity in the plumes, which is not necessarily \hat{U}_c . We are assuming that the spacing between the plumes is ℓ , not unreasonable from figure 10(a). We now balance buoyancy in the thinner thermal layer against viscous drag, omitting the Coriolis term. The Ekman layer is thin, $\sim E^{1/2}$, but at large R the thermal boundary layer is thinner provided the plume local Péclet number $U^* \ell = Pe_\ell^* > E^{-1} \ell^2 \sim E^{-1/3}$ which is more or less true at the highest values of R that we reached. We also note that the conducted flux into the boundary layer scales with $\Delta T'_i / \delta_\kappa$, so

$$R \Delta T'_i \delta_\kappa \sim \frac{U^*}{\delta_\nu}, \quad Nu \sim \frac{\Delta T'_i}{\delta_\kappa}. \tag{4.17a, b}$$

Then (4.16) and (4.17) can be combined to give

$$\Delta T'_i \sim Nu^{4/5} R^{-1/5} \ell^{1/5} P^{-1/10}. \tag{4.17a, b}$$

Since at moderate R , Nu increases linearly with R on the viscous scaling, $\Delta T'_i$ grows as R increases. Our numerics indicate that the temperature drop across the outer boundary $\Delta T'_o$ also grows as R increases. When $\Delta T' = \Delta T'_i + \Delta T'_o$ becomes comparable with γ , this feeds back into (4.15) and slows down the rate of growth of Nu with R . Figure 3 does indeed show that Nu increases more slowly than linearly with R at large R . Ultimately, $\Delta T'$ will be close to γ and the boundary layer will entirely control the heat flux, giving $Nu \sim R^{1/4}$ if ℓ remains constant, though of course at very large R , ℓ may not remain constant. Nevertheless, we certainly expect the boundary-layer regime to lead to a significant drop in the exponent α of the $Nu - 1 \sim (R/R_c - 1)^\alpha$ relation from the value near unity which it has for $R_c < R < 20R_c$. The experiments of Sumita & Olson (2003) gave an exponent of $\alpha = 0.41$ at the highest R they could achieve, suggesting that they were in a regime where the heat transport is controlled by boundary layers, possibly near the tangent cylinder, and that they were not in the moderate- R regime where α is close to unity. Their experiment does not have a fixed tangent cylinder, but allows flow through the tangent cylinder, so the transition layer near the tangent cylinder may have a complex structure.

5. Conclusions

The QGA is a useful model for obtaining insight into the nature of nonlinear rapidly rotating convection outside the tangent cylinder. The picture which has emerged from our numerical solutions of the QGA seems to be generally consistent with the known experimental and theoretical results. The QGA does have some weak points though. There is some uncertainty over how to reduce the temperature equation to two-dimensional form. In our treatment, the QGA imposes a particular latitudinal

distribution of heat flux. An associated problem is that there is no thermal wind in the QGA, that is no zonal flow driven by temperature gradients perpendicular to gravity. In our geometry, with \mathbf{g} in the s -direction, this would require z -variation of T , which is neglected here. Several nonlinear rotating convection experiments have detected the presence of zonal winds. Thermal wind is sometimes suspected, as in the liquid sodium experiment of Shew & Lathrop (2005). However, Aubert *et al.* (2001) showed by direct measurements in their liquid gallium experiment that the thermal wind generated was an order of magnitude less than the observed zonal flow. Possibly the presence of convection inside the tangent cylinder may lead to an enhanced thermal wind. At large P , and possibly also in the presence of magnetic fields with significant Lorentz force, the thermal and magnetic winds may exceed the zonal flow driven by Reynolds stresses.

Weakly nonlinear theory has been shown to be a surprisingly good model for moderate R and large P . Using weakly nonlinear ideas, we have isolated the local Péclet number as a quantity whose R and E dependence follows the weakly nonlinear prediction $Pe_\ell \sim (R\nu/R_c - 1)^{1/2}$ far beyond the mildly supercritical regime. Remarkably, at large values of R_Q , even the low-Prandtl-number results follow this law with a very similar pre-factor to the large- P value.

A number of experiments have found agreement with the inertial scaling of Aubert *et al.* (2001), and the view that at large Rayleigh number results are independent of diffusion was supported by the three-dimensional simulations of Christensen (2002). Our results raise some doubts about the inertial scaling because the Prandtl-number variation does not agree well with our results. Instead, we find that the length scale determined at onset by linear theory still plays an important role even at $R \approx 40R_c$, $P = 7$. It seems that this length scale remains close to the dominant length scale for driving the convection even for strongly supercritical flow. Rather surprisingly, the viscous scaling based on keeping ℓ at its linear critical value seems to do a better job of representing our nonlinear results than the inertial scaling as far as the convective velocity is concerned. It is important to remember that the predicted variation of ℓ with R in the inertial scaling is a very weak $1/5$ power, so that there is not much difference between the inertial and viscous scalings regarding the R and E dependence. It is in the Prandtl-number dependence that the effects of diffusion show up most strongly, as noted by Christensen (2002).

We find, as have others before (e.g. Or & Busse 1987; Tilgner & Busse 1997), that the zonal flow produced by the Reynolds stresses (the thermal wind contribution being outside the scope of the QGA) is stronger and more consistent at low P than at high P . At low P with our no-slip boundary conditions, we find that the dominant balance determining the zonal flow is between the Reynolds stress and the Ekman pumping at the boundary, whereas at high P it is between Reynolds stress and bulk internal dissipation. We find that at large R the zonal flow grows more slowly than the rate $\hat{U}_\phi^0 \sim \hat{U}_c^2$ expected from weakly nonlinear theory if the correlation between u_ϕ and u_s remains at its linear value. We find instead a good fit to the law $\hat{U}_\phi^0 \sim \hat{U}_c^{1.3}$, particularly at low P where the zonal flow is larger and time averages are well-defined. This may be due either to a growth in the radial length scale, as predicted by the inertial scaling with Rhines length given by the zonal flow, or to a progressive decorrelation between u_ϕ and u_s .

The convective heat transport $Nu - 1$ increases approximately linearly with R for moderate $R \leq 10R_c$ at large P , so that the exponent α in the relation $Nu - 1 \sim (R/R_c - 1)^\alpha$ is approximately unity. However, α starts to fall as R is increased further, and in our model this is due to the appearance of thermal boundary layers in which

the Coriolis force is no longer dominant. At large R and small but fixed E we therefore expect the R -dependence of the convective heat transport to become similar to that of boundary-layer-controlled non-rotating convection.

We have not considered here the flow inside the tangent cylinder, or the structure of the layers near the tangent cylinder, which are important features of the full problem. It may be possible to develop a modified form of the QGA to explore convection in these regions, as convection there will still take the form of tall thin columns. However, the weak z -dependence of the z -vorticity, so evident in figure 1(a), is lost; the z -profile of the z -vorticity inside the tangent cylinder has an internal zero, and the z -component of the temperature gradient will also be important there.

We thank Emmanuel Dormy, Dominique Jault, Daniel Brito, Philippe Cardin, Henri-Claude Nataf, Andrew Soward and Keke Zhang for discussion and helpful comments. N.G. is grateful to CNRS and Université Joseph Fourier (Grenoble) for the award of a studentship. C.J. is grateful for the award of PPARC grant PPA/G/S/2001/00129. The computations were performed on the *Service Commun de Calcul Intensif de l'Observatoire de Grenoble*.

REFERENCES

- ARDES, M., BUSSE, F. H. & WICHT, J. 1997 Thermal convection in rotating spherical shells. *Phys. Earth Planet. Inter.* **99**, 55–67.
- AUBERT, J. 2001 Modèles expérimentaux et numériques de la convection dans le noyau de la Terre. PhD thesis, University of Grenoble.
- AUBERT, J., BRITO, D., NATAF, H.-C., CARDIN, P. & MASSON, J. P. 2001 A systematic experimental study of spherical shell convection in water and liquid gallium. *Phys. Earth Planet. Inter.* **128**, 51–74.
- AUBERT, J., GILLET, N. & CARDIN, P. 2003 Quasigeostrophic models of convection in rotating spherical shells. *Geochem. Geophys. Geosys.* **4**, 1052.
- AURNOU, J. & HEIMPEL, M. 2004 Zonal jets in rotating convection with mixed mechanical boundary conditions. *Icarus* **169**, 492–498.
- AZOUNI, M. A., BOLTON, E. W. & BUSSE, F. H. 1986 Convection driven by centrifugal buoyancy in a rotating annulus. *Geophys. Astrophys. Fluid Dyn.* **34**, 301–317.
- BRUMMELL, N. H. & HART, J. E. 1993 High Rayleigh number β -convection. *Geophys. Astrophys. Fluid Dyn.* **68**, 85–114.
- BUSSE, F. H. 1970 Thermal instabilities in rapidly rotating systems. *J. Fluid Mech.* **44**, 441–460.
- BUSSE, F. H. 1986 Asymptotic theory of convection in a rotating, cylindrical annulus. *J. Fluid Mech.* **173**, 545–556.
- BUSSE, F. H. & CARRIGAN, C. R. 1976 Convection induced by centrifugal buoyancy. *J. Fluid Mech.* **62**, 579–592.
- BUSSE, F. H. & OR, A. C. 1986 Convection in a rotating cylindrical annulus: thermal Rossby waves. *J. Fluid Mech.* **166**, 173–187.
- BUSSE, F. H. & SIMITEV, R. 2004 Inertial convection in rotating fluid spheres. *J. Fluid Mech.* **498**, 23–30.
- CARDIN, P. & OLSON, P. 1992 An experimental approach to thermochemical convection in the Earth's core. *Geophys. Res. Lett.* **19**, 1995–1998.
- CARDIN, P. & OLSON, P. 1994 Chaotic thermal convection in a rapidly rotating spherical shell: consequences for flow in the outer core. *Phys. Earth Planet. Inter.* **82**, 235–259.
- CARRIGAN, C. R. & BUSSE, F. H. 1983 An experimental and theoretical investigation of the onset of convection in rotating spherical shells. *J. Fluid Mech.* **126**, 287–305.
- CHRISTENSEN, U. R. 2001 Zonal flow driven by deep convection in the major planets. *Geophys. Res. Lett.* **28**, 2553–2556.
- CHRISTENSEN, U. R. 2002 Zonal flow driven by strongly supercritical convection in rotating spherical shells. *J. Fluid Mech.* **470**, 115–133.

- COLE, S. J. 2004 Nonlinear rapidly rotating spherical convection. PhD thesis, University of Exeter.
- CORDERO, S. 1993 Experiments on convection in a rotating hemispherical shell – transition to chaos. *Geophys. Res. Lett.* **20**, 2587–2590.
- CORDERO, S. & BUSSE, F. H. 1992 Experiments on convection in rotating hemispherical shells: transition to a quasi-periodic state. *Geophys. Res. Lett.* **19**, 733–736.
- DORMY, E., SOWARD, A. M., JONES, C. A., JAULT, D. & CARDIN, P. 2004 The onset of thermal convection in rotating spherical shells. *J. Fluid Mech.* **501**, 43–70.
- GILLET, N., BRITO, D., JAULT, D. & NATAF, H.-C. 2006 Experimental and numerical studies of convection and magnetoconvection in a rapidly rotating spherical shell. *J. Fluid Mech.* (submitted)
- GILMAN, P. A. 1977 Nonlinear dynamics of Boussinesq convection in a deep rotating spherical shell – I. *Geophys. Astrophys. Fluid Dyn.* **8**, 93–135.
- GILMAN, P. A. 1978a Nonlinear dynamics of Boussinesq convection in a deep rotating spherical shell – II: effects of temperature boundary conditions. *Geophys. Astrophys. Fluid Dyn.* **11**, 157–179.
- GILMAN, P. A. 1978b Nonlinear dynamics of Boussinesq convection in a deep rotating spherical shell – III: effects of velocity boundary conditions. *Geophys. Astrophys. Fluid Dyn.* **11**, 181–203.
- GREENSPAN, H. P. 1968 *The Theory of Rotating Fluids*. Cambridge University Press.
- GROTE, E. & BUSSE, F. H. 2001 Dynamics of convection and dynamos in rotating fluid spherical shells. *Fluid Dyn. Res.* **28**, 349–368.
- GUBBINS, D. & ROBERTS, P. H. 1987 Magnetohydrodynamics of the Earth's core. In *Geomagnetism*, Vol. 2 (ed. J. A. Jacobs). Academic.
- HART, J. E., GLATZMAIER, G. A. & TOOMRE, J. 1986 Space-Laboratory and numerical simulations of thermal convection in a rotating hemispherical shell with radial gravity. *J. Fluid Mech.* **173**, 519–544.
- HERRMANN, J. & BUSSE, F. H. 1997 Convection in a rotating cylindrical annulus. Part 4. Modulations and transition to chaos at low Prandtl numbers. *J. Fluid Mech.* **350**, 209–229.
- INGERSOLL, A. P. & POLLARD, D. 1982 Motion in the interiors and atmospheres of Jupiter and Saturn: scale analysis, anelastic equations, barotropic stability criterion. *Icarus* **52**, 62–80.
- JONES, C. A., ROTVIG, J. & ABDULRAHMAN, A. 2003 Multiple jets and zonal flows on Jupiter. *Geophys. Res. Lett.* **30**, Art. 1731.
- JONES, C. A., SOWARD, A. M. & MUSSA, A. I. 2000 The onset of convection in a rapidly rotating sphere. *J. Fluid Mech.* **405**, 157–179.
- MANNEVILLE, J.-B. & OLSON, P. 1996 Banded convection in rotating fluid spheres and the circulation of the Jovian atmosphere. *Icarus* **122**, 242–250.
- MORIN, V. & DORMY, E. 2004 Time dependent β -convection in rapidly rotating spherical shell. *Phys. Fluids* **16**, 1603–1609.
- OR, A. C. & BUSSE, F. H. 1987 Convection in a rotating cylindrical annulus. Part 2. Transitions to asymmetric and vacillating flow. *J. Fluid Mech.* **174**, 313–326.
- PLAUT, E. & BUSSE, F. H. 2002 Low Prandtl number convection in a rotating cylindrical annulus. *J. Fluid Mech.* **464**, 345–363.
- RHINES, P. B. 1975 Wave and turbulence on a beta-plane. *J. Fluid Mech.* **122**, 417–443.
- ROBERTS, P. H. 1968 On the thermal instability of a rotating fluid sphere containing heat sources. *Phil. Trans. R. Soc. Lond. A* **263**, 93–117.
- ROTVIG, J. & JONES, C. A. 2005 Multiple jets and bursting in the rapidly rotating, convecting, 2D annulus model with nearly plane-parallel boundaries. Submitted to *J. Fluid Mech.*
- SALMON, R. 1998 *Lectures on Geophysical Fluid Dynamics*. Oxford University Press.
- SCHAEFFER, N. & CARDIN, P. 2005 Quasi-geostrophic model of the instabilities of the Stewartson layer in flat and depth varying containers. *Phys. Fluids* **17**, 104–111.
- SCHNAUBELT, M. & BUSSE, F. H. 1992 Convection in a rotating cylindrical annulus. Part 3. Vacillating and spatially modulated flows. *J. Fluid Mech.* **245**, 155–173.
- SHEW, W. L. 2004 Liquid sodium model of the Earth's outer core. PhD thesis, University of Maryland.
- SHEW, W. L. & LATHROP, D. P. 2005 Liquid sodium model of geophysical core convection. *Phys. Earth Planet. Inter.* **153**, 136–149.
- SHEW, W. L., SISAN, D. R. & LATHROP, D. 2002 Mechanically forced and thermally driven flows in liquid sodium. *Magnetohydrodynamics* **38**, 121–127.

- SOWARD, A. M. 1977 On the finite amplitude thermal instabilities in a rapidly rotating fluid sphere. *Geophys. Astrophys. Fluid Dyn.* **9**, 9–74.
- SUMITA, I. & OLSON, P. 2000 Laboratory experiments on high Rayleigh number thermal convection in a rapidly rotating hemispherical shell. *Phys. Earth Planet. Inter.* **117**, 153–170.
- SUMITA, I. & OLSON, P. 2003 Experiments on highly supercritical thermal convection in a rapidly rotating hemispherical shell. *J. Fluid Mech.* **492**, 271–287.
- TILGNER, A. & BUSSE, F. H. 1997 Finite-amplitude convection in rotating spherical fluid shells. *J. Fluid Mech.* **332**, 359–376.
- YANO, J.-I. 1992 Asymptotic theory of thermal convection in rapidly rotating systems. *J. Fluid Mech.* **243**, 103–131.
- ZHANG, K. 1992 Spiralling columnar convection in rapidly rotating spherical fluid shells. *J. Fluid Mech.* **236**, 535–556.
- ZHANG, K. 1995 On coupling between the Poincaré equation and the heat equation: non-slip boundary conditions. *J. Fluid Mech.* **284**, 239–256.
- ZHANG, K. & JONES, C. A. 1993 The influence of Ekman boundary layers on rotating convection. *Geophys. Astrophys. Fluid Dyn.* **71**, 145–162.
- ZHANG, K. & LIAO, X. 2004 A new asymptotic method for the analysis of convection in a rapidly rotating sphere. *J. Fluid Mech.* **518**, 319–346.